Oceanographic phenomena caused by interaction of currents and bottom topography – historical notes and theoretical modelling

Ingo Hennings

Over the last few centuries, different structures and colours of the ocean surface have fascinated sailors, fishermen, discoverers, and scientists. Variations of oceanographic parameters caused by the interaction of water currents with bottom topography are summarized based on measurements at different locations of the oceans. Eleven observation areas are presented here which reflect, in particular, the origin from identification, by just watching oceanographic phenomena in relation to the sea bed, until present day theoretical modelling. It is shown that marine remote sensing data are essential for the understanding of different imaging mechanisms in the electromagnetic spectrum. An up to date theory on the radar imaging mechanism of submarine sand waves applying quasi-specular scattering is outlined explaining surface current and bottom topography interaction.

Ozeanographische Phänomene, hervorgerufen durch Wechselwirkung von Strömung und Bodentopographie - historische Aufzeichnungen und theoretische Modellierung. Während der letzten Jahrhunderte haben die unterschiedlichen Strukturen und Farben der Ozeanoberfläche viele Seefahrer, Fischer, Entdecker und Wissenschaftler fasziniert. Es werden Veränderungen von ozeanographischen Parametern, hervorgerufen durch die Wechselwirkung von Strömung mit der Meeresbodentopographie, anhand von Messungen an verschiedenen Stellen des Weltmeeres zusammengefasst. Elf Beobachtungsgebiete werden hier vorgestellt, die besonders die Entwicklung von der Beobachtung und Identifizierung ozeanographischer Phänomene in Verbindung mit dem Meeresboden bis hin zur theoretischen Modellierung beinhalten. Es wird gezeigt, dass marine Fernerkundungsdaten einen wesentlichen Beitrag zum Verständnis der unterschiedlichen Abbildungsmechanismen im elektromagnetischen Spektrum geleistet haben. Eine gegenwärtige Theorie zum Radarabbildungsmechanismus von submarinen Sandwellen wird unter Anwendung von quasi spiegelnder Rückstreuung zur Erklärung der Wechselwirkung zwischen der Oberflächenströmung und Bodentopographie vorgestellt.

1. Introduction

Effects of submarine bottom topography on water properties such as temperature, salinity, and turbidity, as well as ocean dynamics, considering (tidal) current velocity of the surrounding sea in deep and coastal waters, respectively, are subject of past and present research activities. Islanders, sailors, fishermen, discoverers, and seasiders have been known as the first people to describe the different structure and colour of the ocean surface. A study over the last 250 years shows that

many oceanographic phenomena were known, attentively observed, and correctly interpreted when compared with present oceanographic in situ measurements. Under special circumstances, ocean surface currents trace out the shape of underlying sea bottom topography like basins, ridges and plateaus in water depths of the order of hundred and thousand meters. This phenomenon has been referred to as topographic steering which has been known for nearly a century. One example of such striking features is the large-scale ocean circulation within the Nordic Seas and Arctic Ocean with their closed basins known as the Canada Basin, Makarov Basin, Eurasian Basin, Greenland Sea, Lofoten Basin, Norwegian Sea, and Iceland Plateau (Nøst & Isachsen, 2003). It has been observed that the sea bottom topography has a strong effect on water temperature distribution in winter in the East China Sea and Yellow Sea. Observations show that the shallower the water depth is, the lower is the sea surface temperature. As the water depth increases, the surface temperature rises. The reason for this phenomenon is thought to be due to cooling effects by northerly winds during winter. The shallower the ocean is, the volume of water to be cooled is reduced, resulting in more efficient cooling (Tanimoto, 2003).

Today, the classical way of retrieving valuable information on submarine bedforms such as sand waves is the extensive use and analysis of side scan sonar records, including single- as well as multibeam echo sounding data. Sand waves on the continental shelf off Goeree at the Dutch southern North Sea coast seem to have been first recognized 1934 on echo-sounder profiles made from on board the survey vessel *Oceaan* of Rijkswaterstaat, Ministry of Transport, Public Works and Water Management, the Netherlands (Van Veen, 1936; Van Veen, 1938; Kenyon & Stride, 1968; Stolk, 2008). Signatures of normalized radar cross section (NRCS) modulation of marine sand waves were first noticed 35 years later in K_a-band airborne radar imagery acquired on 19 September 1969, one hour before low tide also at the Dutch coast of the southern North Sea (De Loor, 1981).

In this paper the focus is on the variation of oceanographic parameters caused by the interaction of currents with sea bottom topography. In addition, the direct reflection of the sea bed in shallow water without the presence of current variations will also be described using two selected examples. Marine remote sensing data have made a special contribution towards the explanation of the different imaging mechanisms in the visible, infrared and microwave parts of the electromagnetic spectrum. The discovery of nonlinear waves in the ocean's near-surface layer partially caused by irregularities of the sea floor imaged from spaceborne platforms has been summarized by Stevenson (1999). One of the most spectacular and unexpected results of the synthetic aperture radar (SAR) on board the SEASAT satellite flown in space in 1978 was the imaging of sea bottom topography signatures in coastal waters (Alpers & Hennings, 1984; Shuchman et al., 1985). Bandlike patterns appearing to be related to the large submarine sand waves and ridges of Georges Bank at the eastern U.S. North Atlantic coast have been observed by the coastal zone colour scanner (CZCS) on board the Nimbus-7 satellite also launched in space in 1978 (Yentsch et al., 1994). It has always turned out that a strong coherence exists between fluctuations of the oceanic structure and disturbances of

flow velocity. The disturbances of flow velocity are often caused by variations of underwater bottom topography, like seamounts in deep ocean waters and sand banks and sand waves in shallow coastal waters. The presence of water surface roughness changes induced by sea bottom topography structures in coastal waters has also be expected to influence the water surface temperature and might lead to distinctive patterns in remote sensing infrared images.

In the second section different observation sites of the interaction of currents with the sea bottom topography and direct reflection of the sea bed in shallow waters without the presence of current variations are described. One example of an actual developed theory on the radar imaging mechanism of undulations at the sea bed such as marine sand waves using quasi-specular scattering is presented in the third section. Finally, the last section contains a summary.

2. Observation sites

An overview of eleven selected observation sites is presented here reflecting in particular the historical development of observing oceanographic features in the water column and at the sea surface in relation to underwater bottom topography. The locations of the observation sites are shown in Figure 1.

No. 1: Humboldt (1859-1860) made a temperature experiment at the Spanish coast off La Coruña immediately before his research voyage to South America (1799-1804).

No. 2: Chamisso (1995) presented a brief description how the transmittance of sea water was used in the Wotje Atoll for safe navigation in 1817.

No. 3: Möller (1931) showed the influence of the sea bottom relief on the depth positions of boundary layers in the Dardanelles and Bosporus.

No. 4: Defant (1940a) analysed eddies of the Scylla and Charybdis in relation to tidal current velocities in the Strait of Messina.

No. 5: The interaction of oceanographic parameters with the Altair seamount has been described by Defant and Helland-Hansen (1939).

No. 6: Plumes of sea bottom sediments associated with crests of sand waves observed in the sea area between the Sandettie and Outer Ruytingen Banks in the Strait of Dover have been reported by Harden Jones and Mitson (1982).

No. 7: Siegel and Seifert (1985) investigated the influence of the sea bottom on the spectral reflection in the sea area of the Oder Bank in the Baltic Sea.

No. 8: Yentsch et al. (1994) showed colour banding on Georges Bank as viewed by CZCS.

No. 9: Satellite radar and optical visible data of the Norfolk sand banks have been compared by Robinson and Johannessen (1997).

No. 10: Becker (1978) presented airborne infrared scanner data of sea water surface temperature distribution off the isle of Heligoland in the Ger-

man Bight of the North Sea. Multifrequency radar images of the northern sea area off the isle of Heligoland in the German Bight of the North Sea have been analysed by Hennings et al. (1998).

No. 11: Finally, Hennings et al. (2002) studied variations of cold, turbid, and chlorophyll-rich water layers in relation to marine sand waves in the southern North Sea.

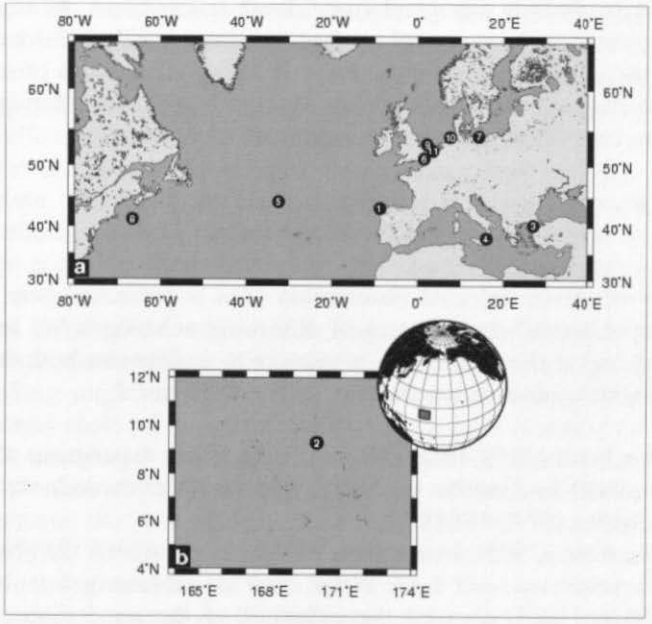

Figure 1: Overview of eleven locations of observation sites worldwide discussed in this paper.

2.1 Entrance to La Coruña (shoal)

Alexander von Humboldt (1769-1859) had already taken much interest on developments in oceanography such as currents, ocean temperature and effects of sand banks. This has been noticed by Carl Böttger (Maury, 1859) in his introduction to the second German edition of Maury's (1855) „The physical geography of the sea". On board the Spanish frigate *Pizarro*, Humboldt (1859-1860) described in the first week of June 1799 an oceanographic phenomenon associated with a shoal at the Spanish Atlantic coast. The location of the observation site is marked as No. 1 in Fig. 1. A part of the hypothetical track of the frigate *Pizarro* passing the shoal with the indicated profile A-B is presented in Figure 2a. A map of the Spanish Atlantic coast from La Coruña to El Ferrol is shown in Figure 2b. On the way from La Coruña to El Ferrol the *Pizarro* probably crossed the shoal Banco Yacentes (Basuril) located at the entrance of the Réa de la Coruña (Bundesamt für

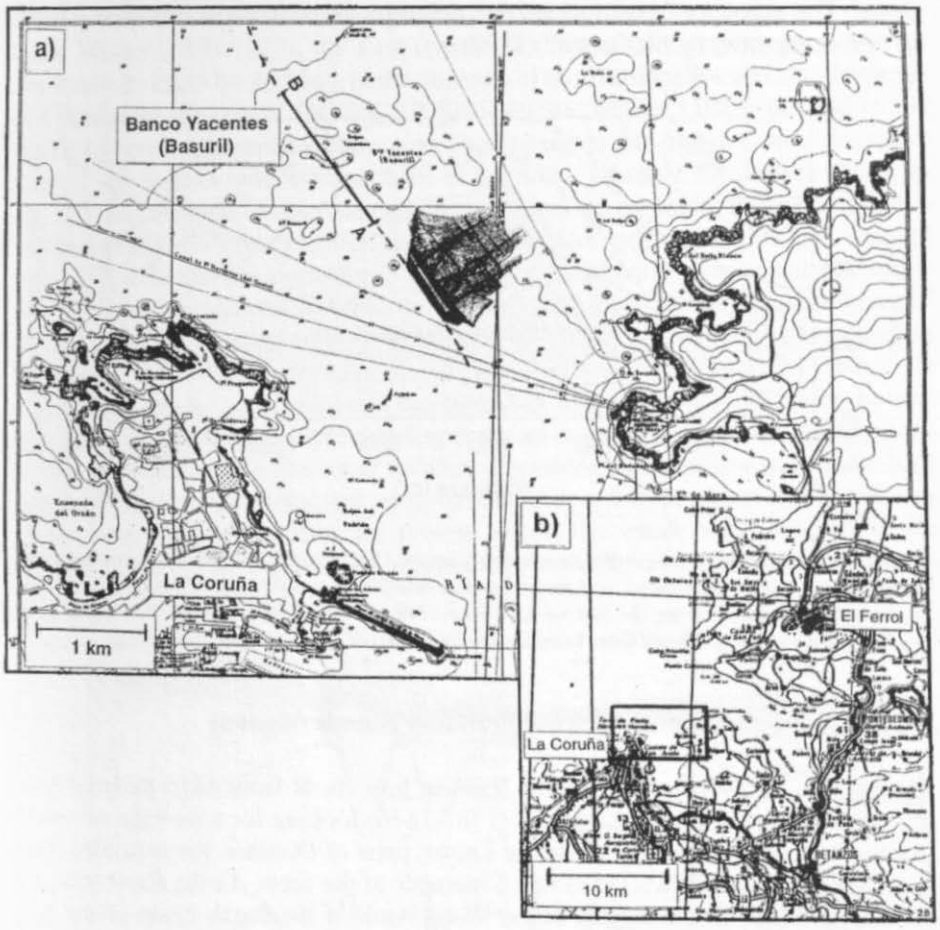

Figure 2: a) Section of a sea chart (Bundesamt für Seeschifffahrt und Hydrographie, 2005) with the location of Banco Yacentes (Basuril) at the entrance to La Coruña, Spain. A reconstructed part of the track of the frigate *Pizarro* passing Banco Yacentes is indicated by the position of profile A-B. b) Overview map of the Spanish coast between La Coruña and El Ferrol with the indicated black frame shown in Fig. 2a.

Seeschifffahrt und Hydrographie, 2005). During this experiment, Humboldt measured a water temperature of 12.5° C - 13.3° C at the sea surface above the bank and of 15.0° C - 15.3° C at the water surface outside the bank in deeper water, respectively. The air temperature was 12.8°. Figure 3 shows the water depth, the sea surface temperature, and the water temperature distribution as a function of water depth across profile A-B (see Fig. 2a for position) according to the measurements and description made by Humboldt. Data obtained from on board cable-ships during the nineteenth century visualized the oceanic thermal regimes globally and in

detail. The existence of cold water above shallow banks was confirmed as a general rule as reported by McConnell (1990)

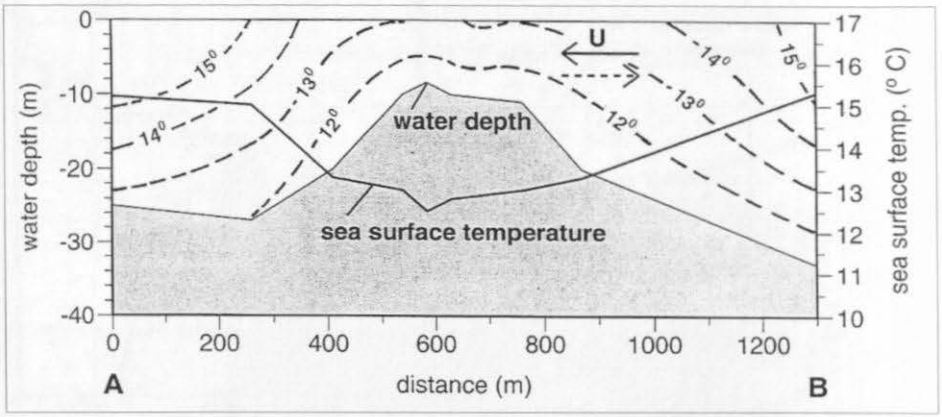

Figure 3: Reconstructed profile A-B across Banco Yacentes (Basuril) (see also Fig. 2a) showing the water depth, the sea surface temperature, and the temperature distribution as a function of water depth according to measurements taken during the first week of June 1799 and the description made by Humboldt. The bold and broken arrows with the letter U indicate the directions of flood and ebb tidal currents.

2.2 Wotje Atoll Marshall Islands (lagoon)

During the discovery voyage of the Russian brig *Rurik* from 1815 to 1818 under the command of Otto von Kotzebue (1787-1846) looking for a passage across the Arctic Ocean and exploring the lesser known parts of Oceania, the naturalist Adalbert von Chamisso (1781-1838) was a member of the crew. As the *Rurik* sailed on 18 January 1817 in the lagoon of the Wotje Atoll of the Ratak chain of the Marshall Islands in the Pacific Ocean from the most western island to the most northern island named Oromed, the captain used the transmittance of sea water for safe navigation (Kotzebue, 1821). „The weather was clear and the bright sun, which shone on the shoals made the plummet dispensable" (English translation), was the statement made by Chamisso (1995). The Wotje Atoll of the Marshall Islands is marked as No. 2 in Fig. 1. The unforeseen appearance of coral reefs arising almost vertically from depth cannot be detected by repeated soundings in time so the captain could not be warned. Its bad visibility at night made such routes in the Pacific Ocean particularly dangerous.

2.3 Dardanelles and Bosporus (sea bottom relief)

Alfred Merz (1880-1925, director of the Institut und Museum für Meereskunde in Berlin before the directorship of A. Defant) had made laborious studies of tidal currents at all depths in the North Sea (Merz, 1921) and of the under-currents

flowing into the Black Sea through the Dardanelles and the Bosporus, Turkey. Lotte Möller (1893-1973), the first female German oceanographer prepared the observations made by A. Merz in the narrows of the Dardanelles and the Bosporus and published the results (Möller, 1928). Later on, Möller (1931) noticed in her publication on „Wasserschichtung und –bewegung in Meerengen" that the influence of sea bottom relief on the depth of boundary layers in the water column itself can be observed along channels in many individual cases. Figure 4 shows a vertical profile of water stratification (potential density) and movement (current velocity) with the position of the „Unterstrommaximum" (under-current maximum), the „Stromgrenze" (current boundary), and the „Grenze der Wasserarten" (boundary of water masses) as a function of water depth through the Dardanelles (Möller, 1931). The observation site of the Dardanelles is marked as No. 3 in Fig.1. In channels and river beds the boundary layers always follow the bottom topography and are spatially extending if numerous eddies with vertical and horizontal axis exist within the water column. Therefore, these eddies must have been generated due to morphological perturbations. According to observations made by Merz, such stationary eddies are present within the whole water column of the Turkish narrows, as the sea bed morphology remains unaltered. New stationary

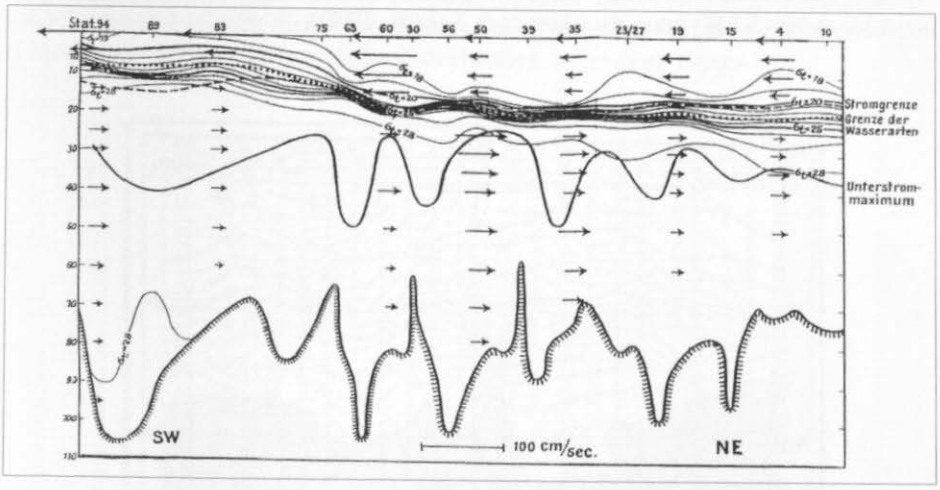

Figure 4: Vertical profile of water stratification (potential density) and movement (current velocity vectors) with the position of the under-current maximum (German: Unterstrommaximum), the current boundary (German: Stromgrenze), and the boundary of water masses (German: Grenze der Wasserarten) as a function of water depth through the Dardanelles, Turkey (Möller, 1931).

eddies can develop in deeper water layers only if sea bottom slopes show formations of corresponding undulations. This description presented by Möller is comparable with recent observations of three-dimensional bed forms such as marine sand waves with sinuous crest lines associated with developing eddies (Hennings & Herbers, 2006).

2.4 Strait of Messina (sea bottom morphology)

„The current velocities and their changes along the Strait of Messina are very interesting to us with regard to the turbulent processes which take place especially at the northern outlet and within the most narrow sector of the strait and which are related to the eddies of Scylla and Charybdis", described the Austrian oceanographer Albert Defant (1884-1974), director of the Institut und Museum für Meereskunde in Berlin 1927-1945, in his publication on Scylla and Charybdis (Defant, 1940a). The location of the Strait of Messina, Italy, is marked as No. 4 in Fig. 1. „Be connected with the current convergences", Defant continues, „are now also eddies with a vertical axis. Here, there exist three locations, which show for their development probably particular favourable morphological sea bottom shapes. These are the locations at Peloro, i.e. the Charybdis, at Scilla, i.e. the Scylla-eddy and the eddy at Punta San Ranieri at the harbour bar of Messina. These eddies have normally a cyclonic rotation. But there exist also such eddies of anticyclonic characters. They are recognizable by their upwelling of water within the central parts. The sea surface appears here as a smooth apparently oily area, why they are also named macchie d'oglio in Italian language". Oceanographic phenomena like Scilla and Charybdis have been also identified in SEASAT synthetic aperture radar (SAR) imagery (Alpers & Salusti, 1983).

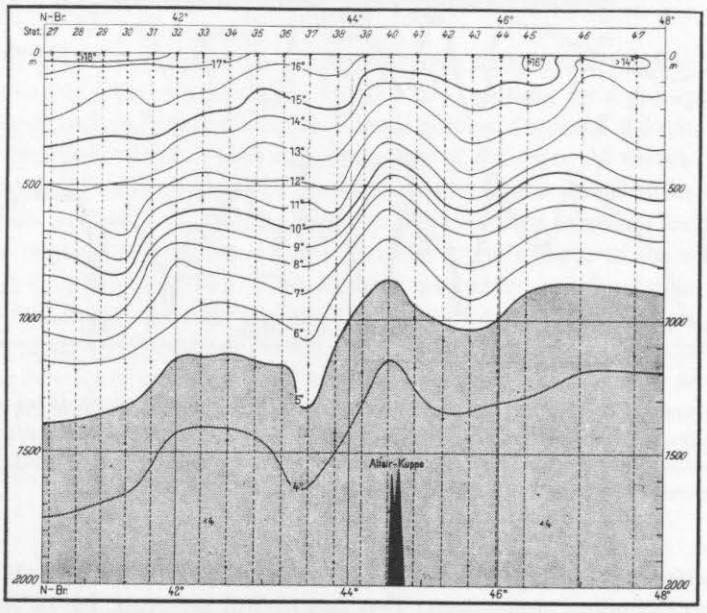

Figure 5: Depth profile of water temperature distribution across the Gulf Stream northwesterly of the Azores measured between 3-6 June 1938 during the International Gulf Stream Expedition (Defant & Helland-Hansen, 1939).

2.5 North Atlantic Ocean (Altair seamount)

The interaction of oceanographic parameters like water temperature and salinity with a seamount due to a current has been observed during the International Gulf Stream Expedition between 31.05.-26.06.1938. This expedition took place in the North Atlantic north-west of the Azores marked as No. 5 in Fig. 1. Defant was chief scientist on board the research vessel *Altair* which was a general cargo freighter chartered by the German Navy. Figures 5-6 show depth profiles of water temperature and salinity distributions, respectively, across the Gulf Stream north westerly of the Azores measured on 3-6 June 1938 (Defant & Helland-Hansen, 1939). Temperature and especially the salinity distributions show wavy disturbances caused at 44.6^0 N in the vicinity of the Altair seamount. A mean depth-averaged residual current velocity of 18 cm s^{-1} with an almost westerly direction has been measured. Defant and Helland-Hansen (1939) assumed that at this location the Gulf Stream was disturbed by the sea bottom topography which was correctly interpreted at that time. But the oceanographic relationships were more complicated as Defant showed in his publication on the oceanographic relations during the anchor station of the *Altair* at the northern boundary of the main flow line of the Gulf Stream north of the Azores (Defant, 1940b). However, these variations in temperature and salinity distributions above a seamount are an impressive example of localized sea bottom topography disturbances in the deep ocean.

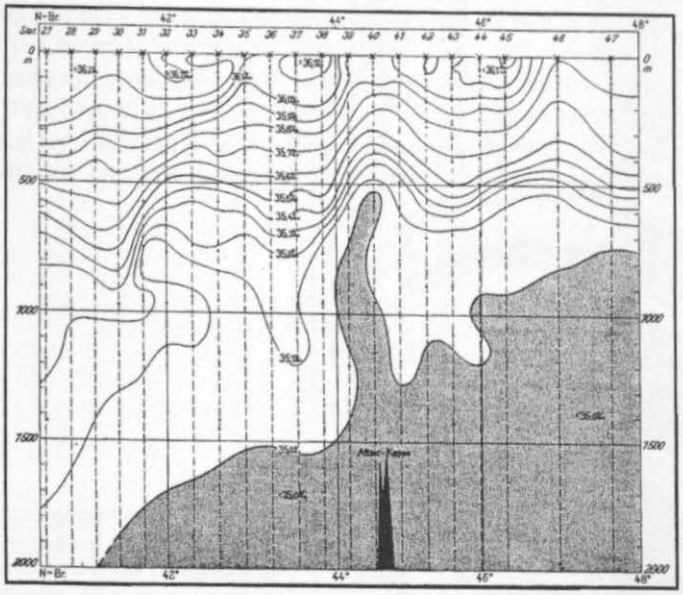

Figure 6: Depth profile of water salinity distribution across the Gulf Stream northwesterly of the Azores measured between 3-6 June 1938 during the International Gulf Stream Expedition (Defant & Helland-Hansen, 1939).

2.6 Strait of Dover (sand waves)

Harden Jones and Mitson (1982) showed that large marine sand waves between the Sandettie and Outer Ruytingen Banks in the Strait of Dover are associated with enhanced acoustical noise levels at their crests. The position of the observation site is marked as No. 6 in Fig.1. The authors called these noise levels „plume-like traces" which have been recorded by 30 kHz and 100 kHz echo sounders as well as by 300 kHz sector-scanning sonar. Figure 7 shows an echo sounder record obtained from on board R.V. *Clione* at 1856 UT - 1909 UT 12 December 1970

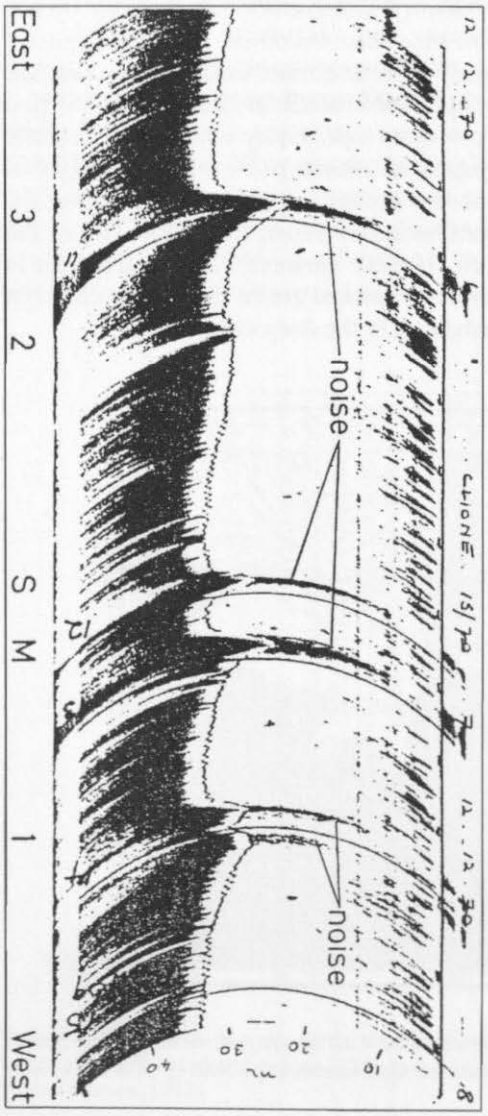

Figure 7: Echo sounder record (KH MS 29, 30 kHz) obtained from on board R.V. *Clione* at 1856 UT-1909 UT 12 December 1970 surveying the sea area between Sandettie and Outer Ruytingen Banks in the southern North Sea showing large sand waves and associated „plumes" of noise (Harden Jones & Mitson, 1982).

surveying the bedforms between the Sandettie and Outer Ruytingen Banks in the southern North Sea. Large sand waves associated with such „plumes" are visible. It was shown that noise from sand waves increases with current velocity. Harden Jones and Mitson (1982) concluded that there exists a relationship between the intensity of measured 300 kHz bottom noise and water current velocity associated with a group of small sand waves located between 150 m - 160 m to the southwest of the Outer Ruytingen anchor station (position: 51° 06.2' N, 1° 53.1' E). Bottom noise and source level are presented as a function of tidal current velocity in Figure 8. The current velocity was measured at 3 m above the sea bottom, water depth below the vessel was 20 m. A wind speed of 6.1 m s^{-1} and a wind direction from 220° were measured. The tidal current direction was northeast. Bottom noise was not detected at velocities less than 0.4 m s^{-1} but was present at higher velocities and increased with the tidal current up to a maximum velocity of 0.91 m s^{-1}. This was an important result because the lower limit of the current velocity of 0.4 m s^{-1} coincides with the lower limit of current velocity for observing a significant NRCS modulation due to marine sand waves (Alpers & Hennings, 1984). Later on, Stolte (1994) reported distinct links between NRCS and sea surface sonar conditions.

Some hypotheses have been discussed that underwater sound sources might be used by fish shoals as indicators of tidal flow or as acoustic beacons by migrants on passage. Harden Jones and Mitson (1982) concluded that the noise was generated by the movement of bottom sediments which might be detected by marine species such as herring and plaice shoals. Stewart and Jordan (1964) observed suspended sediment in the water column just over the crests of submerged sand ridges on Georges Shoal of Georges Bank, Gulf of Maine, USA. During the observations the current direction was normal to the ridge. Shallow water bottom topography from radar imagery and visual evidence of surface expressions of bathymetry at Asia Rip, Phelps Bank, Nantucket Shoals, Massachusetts, USA, have been published by Valenzuela et al. (1983). In aerial photos a pair of light streaks associated with the crests of submerged ridges has been observed also in the sea

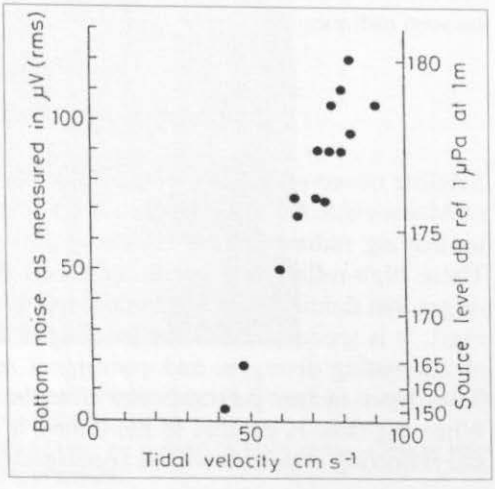

Figure 8: Scatter diagram of the intensity of measured 300 kHz bottom noise and source level associated with a group of small sand waves lying 150 m to 160 m to the southwest of the Outer Ruytingen anchor station (position: 51° 06.2' N, 1° 53.1' E) as a function of tidal current velocity (Harden Jones & Mitson, 1982).

area of Nantucket Shoals (Smith, 1986). It is assumed that these streaks are caused by suspended sediment at large tidal current velocities. The streaks often coincide with a boundary between rough and smooth water at the sea surface. Soulsby et al. (1991) showed that the near bed region above the trough of an asymmetric sand wave in the tidal estuary of the river Taw, southeast England, has the largest values of turbulent kinetic energy, Reynolds stress and sediment concentration. The sand wave trough acts as a source of these parameters. At peak flow no flow separation was visible, but during the decelerating phase, flow reversal has been measured up to 40 % of the time. Until now it has been generally noticed that strong scatter is often detected in regions of the water column expected to be turbulent, but it has never been clear if this is because there are higher plankton or suspended matter concentrations in turbulent regions. Recently, Ross and Lueck (2003) showed that turbulent microstructure strongly scatters sound at 307 kHz.

2.7 Oder Bank (shoal)

The visibility of sea bottom relief on optical satellite images depends on the variation of water surface roughness associated with wind and tidal flow, on the water depth and the reflectivity of the bottom material as well as on the transmission of light through the water column to the sea surface. The latter subject being a highly variable factor because the transmittance may be reduced by suspended material. All of the influences mentioned above often make an interpretation difficult for the mathematical formulation of the optical imaging mechanism. The influence of sea bottom on spectral reflection in the sea area of the Oder Bank in the Baltic Sea has been studied by Siegel and Seifert (1985). The position of the Oder Bank is marked as No. 7 in Fig. 1. The authors noticed bottom reflection up to the surface between 450 nm and 650 nm wavelength of the visible part of the electromagnetic spectrum at the most shallow measurement station of 8 m water depth. Indeed, the sea area of the Oder Bank has been often detected in CZCS satellite images by enhanced radiance.

2.8 Georges Bank (sand waves and ridges)

Satellite observations of Georges Bank located at the eastern North Atlantic coast of Maine (U.S.A.) made by the CZCS sensor showed bandlike patterns in the water-leaving radiance most visible at 550 nm wavelength (Yentsch et al., 1994). These high-reflectance bands appear to be related to the large sand waves and ridges that dominate the sea bottom topography at that location marked as No. 8 in Fig.1. It is speculated that the banding in the CZCS data is caused by the creation of alternating divergent and convergent zones due to tidal currents as the water flows more or less perpendicular over the underwater dune-trough configuration. When the flow is parallel to the dunes, it is speculated that suspended absorbing and reflecting materials will be concentrated by helical vortices.

2.9 Norfolk Banks (tidal current ridges)

Robinson and Johannessen (1997) described European remote sensing satellite (ERS-1) SAR and ERS-2 along-track scanning radiometer (ATSR-2) images from the southern North Sea, off the north Norfolk coast of the United Kingdom. The position of the satellite imagery is marked as No. 9 in Fig. 1 but is not shown here. Acquisition time of the SAR scene was at 1051 UT 21 October 1995 and the ATSR-2 image was acquired 30 minutes later. The bathymetry consists of a number of linear tidal current ridges approximately parallel to the coast. Significant SAR signatures have been caused by tidal flow over the ridges modulating the sea surface roughness. The corresponding ATSR-2 550 nm wavelength reflectance image shows also an enhanced reflectance over the banks. It is well known that North Sea water is far too turbid for this to be reflection from the sea bed, and the most likely explanation is that suspended sediment concentration is enhanced over the banks.

2.10 Heligoland, German Bight (reefs)

Sea surface temperature distribution off the isle of Heligoland in the German Bight of the North Sea was acquired by an airborne infrared scanner (Becker, 1978). The investigated area is indicated as No. 10 in Fig. 1. The image acquired

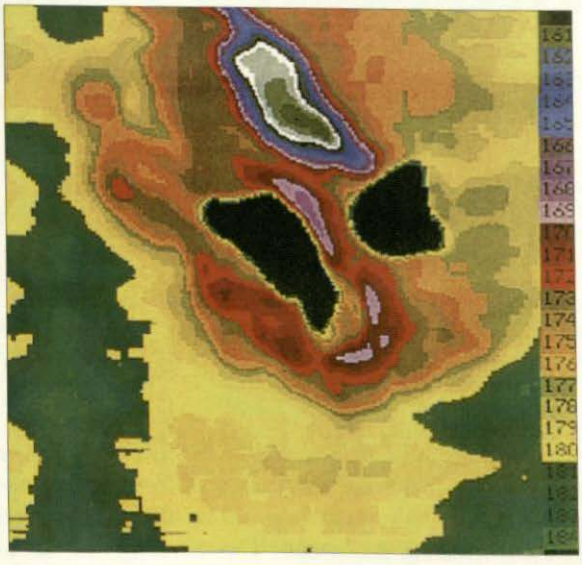

Figure 9a: Two-dimensional water surface temperature distribution around Heligoland at 1506 UT 29 August 1976 acquired by an airborne infrared scanner (Becker, 1978).
The isle of Heligoland and the shallow island, called Dune, are marked by black colour. Contour lines of both islands are blurred due to numerical filtering processes.

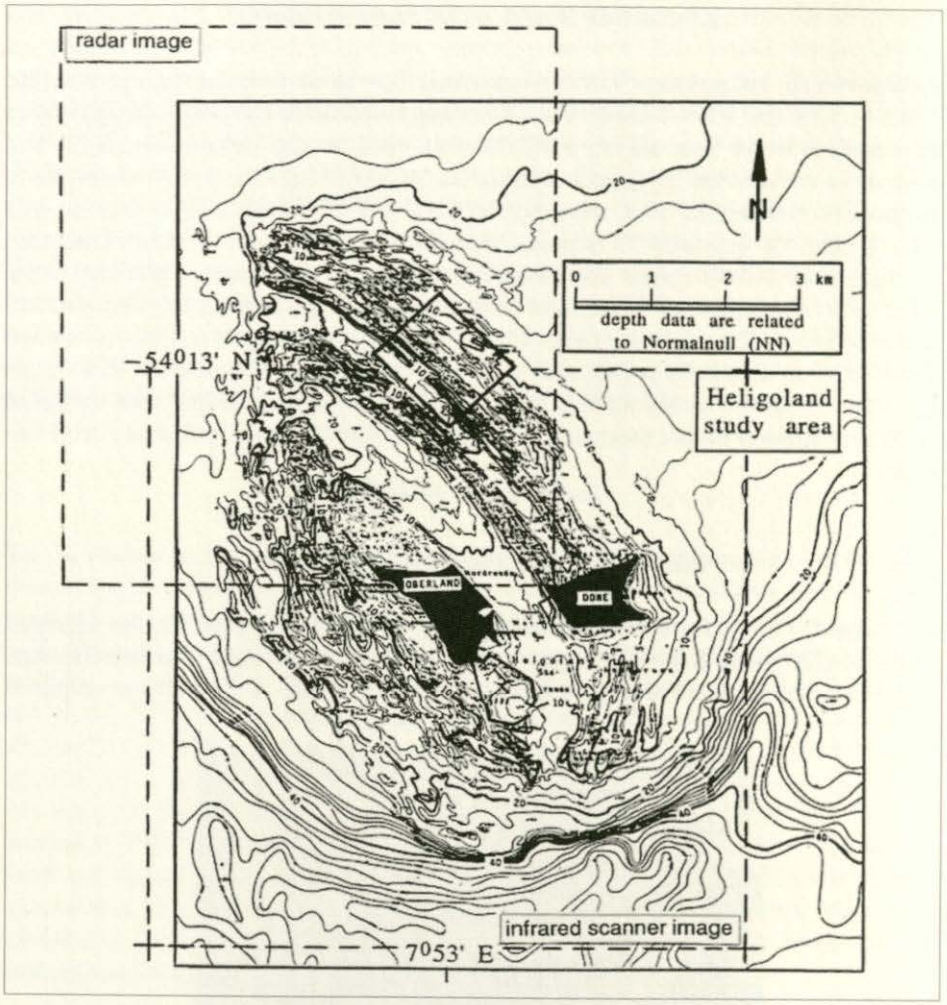

Figure 9b: Bathymetric chart of the sea area around Heligoland (Kuratorium für Forschung im Küsteningenieurwesen, 1977a, b). Depth contours are in meters. The larger broken frame is the area covered by the infrared scanner image presented in Fig. 9a and the smaller broken frame indicates the coverage of the SAR image shown in Fig. 9c.

at 1506 UT 29 August 1976 is shown in Figure 9a and indicates remarkable two-dimensional temperature gradients in north-south as well as in east-west direction. Original spatial resolution of the image was 10 m but has been reduced to about 67 m due to numerical filtering processes. The coverage of the infrared scanner image is indicated by the larger broken frame in Fig. 9b. The data were taken one hour after high water at Heligoland during ebb tidal phase. The tidal current speed varied between 10 cm s^{-1} and 30 cm s^{-1} and northerly tidal current directions. The wind speed was 3 m s^{-1} and the wind direction was from 90^0. Above the shal-

low sea area north-west of the island called Dune the lowest water temperatures < 15.7° C were recorded. It is assumed that bottom water from the westerly sea area of the shoals was almost transported unmixed above the shallow parts of the sea area. Becker (1978) concluded that this phenomenon may be attributed to current conditions depending on tidal phase and local bathymetry of the sea area. A bathymetric chart of the sea area around Heligoland is shown in Figure 9b (Kuratorium für Forschung im Küsteningenieurwesen, 1977a, 1977b).

Multifrequency X-, C-, and L-band SAR images north of the sea area off the isle of Heligoland were analysed by Hennings et al. (1998). The coverage of the SAR image is indicated by the smaller broken frame in Fig. 9b. The data have been collected during the SAR and X-band Ocean Nonlinearities Research Platform North Sea Experiment (SAXON-FPN) at 0644 UT 14 November 1990. Figure 9c is the result of the superposition of the X- and L-band SAR images. The X-band VV polarized SAR image is processed in red colour and the L-band VV polarized SAR image is processed in blue colour, respectively. Features appearing in black and white have not changed their characteristics in their X- and L-band frequency domain and coloured signatures show differences. Elongated streaks of predominantly low radar return are related to near-shore reefs (see Fig. 9b) and are

Figure 9c: Multi-frequency SAR image of the sea area of Heligoland, German Bight, south eastern North Sea at 0644 UT 14 November 1990. The X-band VV polarized SAR image is processed in red colour and the L-band VV polarized SAR image is processed in blue colour, respectively. Features appearing in black and white have not changed their characteristics in the X- and L-band frequency domain. Coloured signatures show changes of the environment.

imaged on all multifrequency radar scenes. Ground resolution in range and azimuthal direction of the SAR image is 5 m. The data were taken 1 hour and 56 minutes before high water at Heligoland during flood tidal phase with a mean tidal current speed of 0.6 m s^{-1} and a mean tidal current direction of 98^0. The wind speed was 9 m s^{-1} and the wind direction was from 200^0.

2.11 Southern Bight of the North Sea (sand waves)

A similar effect of cold water flowing across shallow banks and reefs as described in section 2.1 is here associated with marine sand waves and has been measured in the sea area of the Southern Bight of the North Sea (Hennings et al., 2002). The location of the observation site is marked as No. 11 in Fig. 1. Quasi-periodic vari-

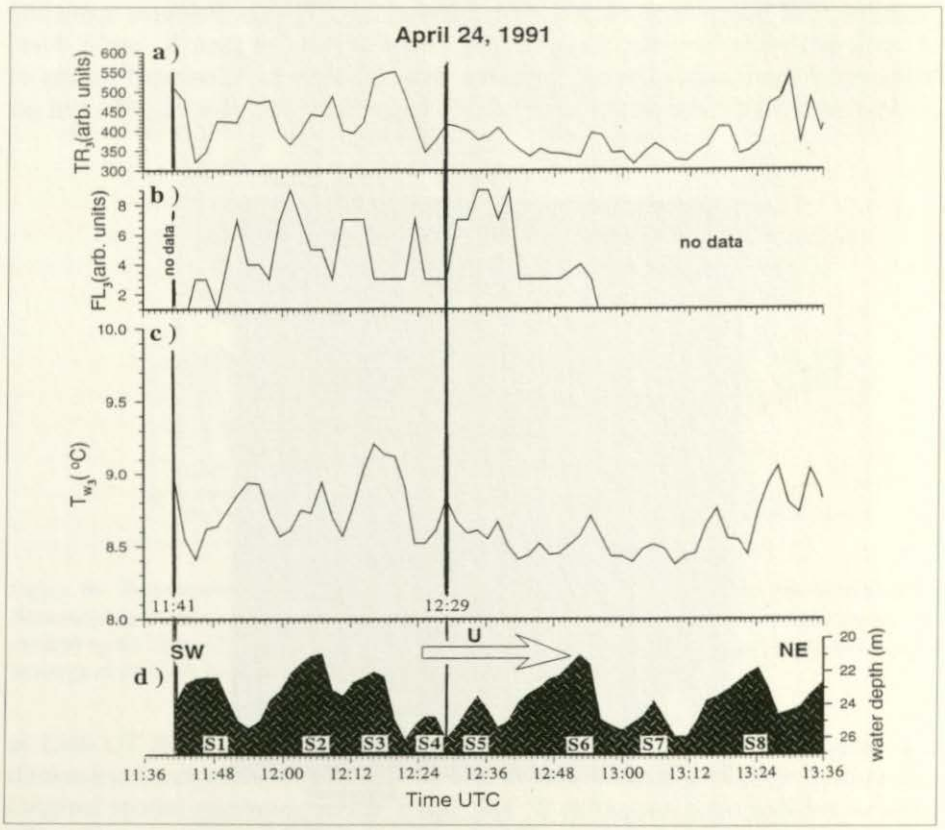

Figure 10: Time series of a) beam transmittance TR_3 (arbitrary units), b) fluorescence FL_3 (arbitrary units), and c) water temperature $T_{W\ 3}$ (^{0}C) at 3 m water depth in relation to d) water depth profile between 1141 UT-1336 UT 24 April 1991. Each tick mark indicates one minute. The direction of the tidal current U is indicated by a white arrow in Fig. 10d. The investigations have been carried out in the southern North Sea where the sea bed is covered by sand waves numbered by S1-S8 (Hennings et al. 2002).

ations in beam transmittance TR_3, fluorescence FL_3, and water temperature $T_{W\,3}$ at 3 m water depth in relation to the water depth profile of the drift path A-B at 1141 UT - 1336 UT 24 April 1991 are shown in Figure 10. Cold, turbid, and chlorophyll-rich water from greater water depths below the thermocline arrived prior to the marine sand wave crests and just before the current velocity was at a maximum. This mechanism has been explained as quasi resonant internal waves with marine sand waves (Hennings et al., 2002).

The reason why Humboldt measured lower water temperature on the bank than in deeper surrounding waters (see section 2.1) could be due to the presence of a tidal current flow. If this is assumed, then a similar effect as has been observed above the marine sand waves at the Dutch coast in the southern North Sea can arise at the Banco Yacentes. In that sea area there can also be an overflow of colder water from deeper water depths above a shoaling sea bed induced by tidal currents (see also section 2.10).

3. Quasi-specular scattering theory

The creation of alternating divergent and convergent zones caused by (tidal) currents as the water flows over a wavy sea bed configuration and its radar imaging mechanism belonging to the microwave part of the electromagnetic spectrum will be outlined here as an example. The formulated theory is applicable to the X-band SAR of TerraSAR-X, Germany's first civil national remote sensing satellite realized by a public-private partnership. Radar signatures of sea bottom topography are dominated by Bragg scattering since most of the imaging radars operate at incidence angles between 20° and 70° (Valenzuela, 1978). At low radar incidence angles, < 20°, quasi-specular scattering dominates. In addition, quasi-specular scattering becomes dominant at higher radar frequencies. According to Bragg scattering theory, the NRCS for small water surface waves is proportional to the wave height spectral density at the Bragg backscatter wave numbers. For quasi-specular scattering from a rough ocean surface, the NRCS is proportional to the total variance of slopes created by ocean surface waves. The radar imaging mechanism of sea bottom topography depends strongly on radar incidence angle, radar frequency, radar polarization, current speed and -direction, as well as wind speed and -direction. The most important assumption for the radar imaging mechanism of submarine bedforms is the presence of strong currents, preferably tidal currents ≥ 0.5 m s^{-1} at wind speeds ≤ 8 m s^{-1}. Specular reflection occurs when radiation is scattered into a given direction from surface regions with slopes such that the local specular direction coincides with the scattering direction. The quasi-specular scattering theory can be applied if the wavelengths of waves in the ocean contributing to the mean square surface slope are greater than the wavelength of the microwave. In general, the mean squared slope of such waves is small. But this is considerably different if waves are influenced by a surface current gradient. Very steep disturbed slopes of the order of 10° or more can arise in the convergence zone of the current correlated with the slope regions of marine sand waves. Water

waves especially of trochoidal shape, can be generated due to such wave-current interaction at low to moderate wind speeds. These trochoidal shaped waves produce an ensemble average of facets which create quasi perpendicular planes relative to the transmitted radar beam. There exist also steep small gravity waves in this zone which tend to become sharp wedges just before they break, and also breaking waves themselves. Improvements of the quasi-specular scattering theory have to be made because the radar imaging mechanism of the sea bed depends strongly also on the up- and crosswind wave slopes, the angle between the upwind and perpendicular current direction to the sand wave crest, and the angle between the radar range direction and the upwind direction.

The disturbed NRCS $\delta\sigma_{dis}$ caused by the disturbance of the surface current $\delta U(\vec{x})$ due to marine sand waves based on quasi-specular scattering and obeying a Gram-Charlier series is given by (Hennings & Herbers, 2007)

$$\delta\sigma_{dis} = \sigma - \sigma_0 = \pi\left|R(0)\right|^2 \sec^4(\theta_0 + \delta\theta)\, p\left(\zeta_{x_0} + \delta\zeta_x, \zeta_{y_0} + \delta\zeta_y\right) - \sigma_0 \qquad (1)$$

where σ is the local NRCS influenced by the disturbance of $\delta U(\vec{x})$, σ_0 is the background NRCS, $R(0)$ is the Fresnel reflection coefficient at normal incidence, θ_0 is the angle of incidence, $\delta\theta$ is the time-dependent perturbation term of the incidence angle, $\zeta_{x_0} = \partial\zeta_0/\partial x$ and $\zeta_{y_0} = \partial\zeta_0/\partial y$ are the slopes of the rough sea surface in two orthogonal directions, x and y, ζ_0 is the vertical elevation of the sea surface, $\delta\zeta_x$ and $\delta\zeta_y$ are the time-dependent perturbation terms of ζ_{x0} and ζ_{y0} in two orthogonal directions, x and y respectively.

The local joint-probability density function of slopes expressed in equation (1) is defined by

$$\begin{aligned} p\left(\zeta_{x_0} + \delta\zeta_x, \zeta_{y_0} + \delta\zeta_y\right) \approx \frac{1}{2\pi\sigma_u\sigma_c}\left\{\exp\left[-\frac{1}{2}\left(s_u^2 + s_c^2\right)\right]\right\} \\ \left\{1 - \left(\frac{1}{2}\right)c_{21}\left(s_c^2 - 1\right)\right. \\ -\left(\frac{1}{6}\right)c_{03}\left(s_u^3 - 3s_u\right) + \left(\frac{1}{4}\right)c_{22}\left(s_c^2 - 1\right)\left(s_u^2 - 1\right) \\ \left.+\left(\frac{1}{24}\right)\left[\, c_{40}\left(s_c^4 - 6s_c^2 + 3\right) + c_{04}\left(s_u^4 - 6s_u^2 + 3\right)\right]\right\} \end{aligned} \qquad (2)$$

where σ_u and σ_c are the local standard deviations of the upwind and crosswind wave slopes, s_u^2 and s_c^2 are the squared local normalized upwind and crosswind wave slopes, c_{21} and c_{03} are the skewness coefficients as a function of the wind speed u_w, and c_{40}, c_{22}, and c_{04} are constant peakedness coefficients (Cox & Munk, 1954). The probability distribution function for sea surface slopes as a function of wind direction is skewed, and displaced from zero in the upwind-downwind direction. The peak of distribution in wind direction is shifted toward

the downwind side by several degrees. This is due to the fact that the longer gravity waves tend to have a higher spectral wave energy density of short waves on their downwind faces than in their troughs or upwind faces (Apel, 1987).

The square tangent of the disturbed incidence angle in equation (1) is derived by

$$\tan^2\delta\theta = +\delta\theta^2 = \delta\sigma_u^2 + \delta\sigma_c^2 \quad , \quad \frac{\partial u_{perp}}{\partial x_{perp}} \leq 0 \tag{3a}$$

and

$$-\tan^2\delta\theta = -\delta\sigma^2 = -\left(\delta\sigma_u^2 + \delta\sigma_c^2\right) \quad , \quad \frac{\partial u_{perp}}{\partial x_{perp}} > 0 \tag{3b}$$

with

$$\delta\sigma_u^2 = \int_{k_0}^{k} \vec{k}^2\left(\vec{x}\right)\delta F\left(\vec{x},\vec{k}\right)\cos\alpha \, d\vec{k} \tag{4a}$$

and

$$\delta\sigma_c^2 = \int_{k_0}^{k} \vec{k}^2\left(\vec{x}\right)\delta F\left(\vec{x},\vec{k}\right)\sin\alpha \, d\vec{k} \tag{4b}$$

where x_{perp} is the space variable defined perpendicular to the sand wave crest, $\vec{k}$ is the wave number vector of short gravity waves, k_0 is the lower limit of the wave number producing quasi-specular scattering modulation, k_c is the maximum wave number neglecting the effect of surface tension, du_{perp}/dx_{perp} is the gradient or strain rate of the current velocity perpendicular to the sand wave crest, α is the angle between the upwind direction and the current velocity component perpendicular to the sand wave crest, and $\delta F\left(\vec{x},k\right)$ is the perturbation term of the wave energy density spectrum in the short gravity wave regime caused by wave-current interaction applying weak hydrodynamic interaction theory (Alpers & Hasselmann, 1978).

The relationship between $\psi\left(\vec{k}\right)$, $F\left(\vec{k}\right)$ and the wave action density spectrum $N\left(\vec{k}\right) = F\left(\vec{k}\right)\left(\omega'(k)\right)^{-1}$ is defined by (Holliday et al., 1986)

$$F\left(\vec{k}\right) = \omega'(k)N\left(\vec{k}\right) = \frac{\omega'(k)^2}{k}\psi\left(\vec{k}\right) \tag{5}$$

with the wave height spectrum

$$\psi(k) = a_p k^{-4} \tag{6}$$

where a_P is known as the Phillips constant. Based on measurements by Stolte (1990), the empirical relation for a_P as a function of wind speed ≤ 8 m s^{-1} is used

$$\log_{10} a_p = -2.90 + 3.06\cdot 10^{-1} u_w - 1.85\cdot 10^{-2} u_w^2 \tag{7}$$

The intrinsic angular wave-frequency for gravity waves in equation (5) is defined by

$$\omega' = (gk)^{1/2} \tag{8}$$

For the modulation of the first order perturbed wave-energy density spectrum $\delta F / F_0 = (F - F_0)/F_0$ (with F_0 as the unperturbed wave-energy density spectrum) the expression derived by Alpers and Hennings (1984) is used

$$\frac{\delta F}{F_0} = -4.5 \frac{\partial u_{\text{perp}}}{\partial x_{\text{perp}}} \left(\left(\vec{c_g} + \vec{u_0} \right) \frac{1}{\text{L}} + \mu \right)^{-1} \tag{9}$$

with the absolute value of the group velocity for gravity waves

$$\left| \vec{c_g} \right| = \frac{1}{2} \frac{\omega'}{k} \tag{10}$$

where $\vec{u}_0$ is the mean current velocity of the undisturbed sea area, μ is the relaxation rate parameter, g is the acceleration of gravity, $\text{L} = \text{L}_{\text{SSL}}$ is the length scale of the steep slope, and $\text{L} = \text{L}_{\text{GSL}}$ is the length scale of the gentle slope of the sand wave, respectively.

Relation (9) shows that the first-order perturbed wavenumber spectrum of short gravity waves is proportional to the current gradient caused by marine sand waves. This is an important result. As a first approximation, using the continuity equation, this, in turn, is proportional to the sea bottom slope divided by the square of the water depth. Consistently, the spectral wave energy density of the scattered waves, and thus the intensity of the radar signal, is largest on the downstream side of the sand wave or ridge and smallest on the upstream side. As a consequence, when the current flows in opposite directions during the ebb and flood of the tide, a sign reversal of the image intensity is expected, which is indeed observed in radar images (Zimmerman, 1985). A detailed background of the weak hydrodynamic interaction theory for the radar imaging mechanism of the sea bed is given in Alpers and Hennings (1984) and Hennings and Herbers (2006).

The same hydrodynamic interaction mechanism described above for the radar imaging theory is also responsible for surface manifestations of oceanographic phenomena in the optical visible part of the electromagnetic spectrum. Variations in water temperature and chlorophyll distributions reflect also the influence of sea bottom topography undulations because tidal flow over wavy sea bed configurations produces alternating divergent and convergent regions. It can often be observed that the tidal flow is not of barotropic character near the crests and troughs of marine sand waves. This implies that mass is not only conserved by an acceleration or deceleration of the flow but that up- and downwelling of the three-dimensional current field can also play a significant role. Yentsch et al. (1994) considered that the biological importance of these features concerns the process of new production and the off-bank transport of inorganic and organic materials (see also section 2.8).

4. Summary

Observation sites concerning variations of oceanographic parameters caused by the interaction of currents with sea bottom topography over the period of the last 250 years are described. The development from simple observing and measuring tools of physical parameters within the water column to its mathematical formulation for understanding the dynamical processes has been shown. Oceanographic parameters like sea surface temperature, ocean colour, slope, and sea surface roughness with their specific variations have often been used to investigate and describe the ocean dynamics influenced by characteristic features of the sea bed. Sea surface temperature variations associated with a shallow submarine bank at the entrance to La Coruña at the Spanish coast of the Atlantic Ocean was measured by Humboldt in 1799. These measurements of Humboldt have been confirmed for example by observing similar effects 1976 above shallow reefs off the isle of Heligoland imaging sea surface temperature and 1991 in the southern North Sea measuring water quality parameter variations at a water depth of 3 m above marine sand waves. For most of these observations a strong (tidal) current is required as the dominant source to observe any variation or modulation of oceanographic parameters.

It has been shown that shore- and ship-based as well as air- and spaceborne marine remote sensing measurement configurations promised considerable improvements in quality and synopsis of field data. High spatial and radiometric resolution data have been acquired and have opened new horizons in basic research. Thermal inhomogeneities developing at calm or low wind speed of 2-3 m s^{-1} have been referred as „calm weather thermal inhomogeneities" (Fedorov, 1986) where sea surface signatures are often imaged in the visible part of the electromagnetic spectrum. The mechanism of its formation can easily be visualized in the case of a monochromatic internal wave. Orbital motions, which become horizontal alternating convergent-divergent flows at the sea surface, form accumulations of passive constituents, solar-heated water and surface-active material in the convergence zones.

Nowadays, the investigation of oceanographic phenomena is coupled with its mathematical formulations. In summary, if the microwave part of the electromagnetic spectrum is considered here, then the radar imaging mechanism of submarine sand waves can be physically and mathematically described as a process consisting of at least three steps (see also section 3): 1) The interaction between the current and the sea bottom topography produces variations in the current velocity at the sea surface. 2) The variation of the surface current modulates the short-scale sea surface roughness which can be described by the weak hydrodynamic interaction theory in the relaxation time approximation. 3) The disturbed variance of slopes of short ocean surface waves via the modulation of the spectral wave energy density at the water-air boundary layer gives rise to changes in radar backscatter.

Acknowledgement

M. Plettendorff of the library at the Bundesamt für Seeschifffahrt und Hydrographie, Hamburg, Germany, is gratefully acknowledged for the scanning of the airborne infrared scanner image published by Becker (1978). I would like to thank J. Evans-Morgis of the Naval Air Development Center for providing the SAR imagery, C. Wackerman, Environmental Research Institute of Michigan, for processing the SAR images, and M. Metzner for technical support.

References

Alpers, W. & K. Hasselmann, 1978. The two-frequency microwave technique for measuring ocean wave spectra from an airplane or satellite. Boundary-Layer Meteorology, 13: 215-230.

Alpers, W. & E. Salusti, 1983. Scylla and Charybdis observed from space. Journal of Geophysical Research, 88 (C6): 1800-1808.

Alpers, W. & I. Hennings, 1984. A theory of the imaging mechanism of underwater bottom topography by real and synthetic aperture radar. Journal of Geophysical Research, 89 (C6): 10529-10546.

Apel, J.R., 1987. Principles of ocean physics. Academic Press, London, 634 pp.

Becker, G.A., 1978. Infrarot-Scanner-Aufnahme der Wassertemperatur um Helgoland. Deutsche Hydrographische Zeitschrift 31: 105-106.

Bundesamt für Seeschifffahrt und Hydrographie, 2005. Seekarte No. 615, Cabo Prior bis Punta Langosteira, Hamburg.

Chamisso, A. v., 1995. Reise um die Welt mit der Romanzoffischen Entdeckungs-Expedition in den Jahren 1815-18 auf der Brigg Rurik. Gondrom Verlag GmbH & Co. KG, Bindlach, 95-511.

Cox, C. & W. Munk, 1954. Measurement of the roughness of the sea surface from photographs of the sun's glitter. Journal of the Optical Society of America 44: 838-850.

Defant, A. & Bj. Helland-Hansen, 1939. Bericht über die ozeanographischen Untersuchungen im zentralen und östlichen Teil des Nordatlantischen Ozeans im Frühsommer 1938 (Internationale Golfstrom-Expedition). Abhandlungen der Preußischen Akademie der Wissenschaften, Physikalisch-mathematische Klasse, Nr. 5, Verlag der Akademie der Wissenschaften in Kommission bei Walter de Gruyter u. Co., Berlin, 64 pp.

Defant, A., 1940a. Scylla und Charybdis und die Gezeitenströmungen in der Straße von Messina. Annalen der Hydrographie und Maritimen Meteorologie 68: 145-157.

Defant, A., 1940b. Die ozeanographischen Verhältnisse während der Ankerstation des „Altair" am Nordrand des Hauptstromstriches des Golfstromes nördlich der Azoren (44^0 33' N-Br., 38^0 58' W-Lg., 16. bis 20. Juni 1938). Annalen der Hydrographie und Maritimen Meteorologie (November-Beiheft) 68: 35 pp.

De Loor, G.P., 1981. The observation of tidal patterns, currents and bathymetry with SLAR imagery of the sea. IEEE Journal of Oceanic Engineering 6: 124-129.

Fedorov, K.N., 1986. The physical nature and structure of oceanic fronts (vol. 19 of Lecture notes on coastal and estuarine studies). Springer-Verlag, Berlin, 333 pp.

Harden Jones, F.R. & R.B. Mitson, 1982. The movement of noisy sandwaves in the Strait of Dover. Journal du Conseil/Conseil Permanent International pour l'Exploration de la Mer 40(1): 53-61.

Hennings, I., M. Metzner & C.J. Calkoen, 1998. Island connected sea bed signatures observed by multi-frequency synthetic aperture radar. International Journal of Remote Sensing 19: 1933-1951.

Hennings, I., M. Metzner & G.-P. De Loor, 2002. The influence of quasi resonant internal waves on the radar imaging mechanism of shallow sea bottom topography. Oceanologica Acta 25: 87-99.

Hennings, I. & D. Herbers, 2006. Radar imaging mechanism of marine sand waves at very low grazing angle illumination caused by unique hydrodynamic interactions. Journal of Geophysical Research 111: C10008, doi: 10.1029/2005JC003302.

Hennings, I. & D. Herbers, 2007. The expected potential of TerraSAR-X high resolution spotlight mode data for shallow sea bottom topography imaging: a preview. EARSeL eProceedings 6(2): 67-81.

Holliday, D., G. St-Cyr & N.E. Woods, 1986. A radar ocean imaging model for a small to moderate incidence angles. International Journal of Remote Sensing 7: 1809-1834.

Humboldt, A. v., 1859-1860. Reise in die Aequinoctialgegenden des neuen Continents. In deutscher Bearbeitung von H. Hauff, Vol. 1-4, J.G. Cotta, Stuttgart, XIII, 403, 416, 403, 444 pp.

Kenyon, N.H. & A.H. Stride, 1968. The crest length and sinuosity of some marine sand waves. Journal of Sedimentary Research 38: 255-259.

Kotzebue, O. v., 1821. Entdeckungs-Reise in die Süd-See und nach der Bering-Straße zur Erforschung einer nordöstlichen Durchfahrt. Unternommen in den Jahren 1815, 1816, 1817 und 1818, auf Kosten Sr. Erlaucht des Herrn Reichs-Kanzlers Grafen Romanzoff auf dem Schiffe Rurik. Weimar, Band 1.

Kuratorium für Forschung im Küsteningenieurwesen, 1977a. Coastal Chart 1712 K Sellebrunn, Kiel, Germany.

Kuratorium für Forschung im Küsteningenieurwesen, 1977b. Coastal Chart 1812 K Helgoland, Kiel, Germany.

Maury, M.F., 1855. The physical geography of the sea. Harper & Brothers, New York, XV, 274 pp.

Maury, M.F., 1859. Die physische Geographie des Meeres, in deutsch bearbeitet von C. Böttger, 2., mehrfach veränderte und vermehrte Auflage, Gustav Mayer, Leipzig, XV, 294 pp.

McConnel, A., 1990. The art of submarine cable-laying: its contribution to physical oceanography. In: Ocean sciences: their history and relation to man, proceedings of the 4th International Congress on the History of Oceanography, Hamburg 23.-29.09.1987, edited by W. Lenz and M. Deacon, Deutsche Hydrographische Zeitschrift, Ergänzungsheft, Reihe B, No. 22, 467-473.

Merz, A., 1921. Gezeitenforschungen in der Nordsee. Annalen der Hydrographie und Maritimen Meteorologie 49: 393-400.

Möller, L., 1928. Alfred Merz hydrographische Untersuchungen in Bosporus und Dardanellen. Veröffentlichungen des Instituts für Meereskunde an der Universität Berlin, Neue Folge, A, 18, 284 pp.

Möller, L., 1931. Wasserschichtung und –bewegung in Meerengen. Annalen der Hydrographie und Maritimen Meteorologie 59: 7-17.

Nøst, O.A. & P.E. Isachsen, 2003. The large-scale time-mean ocean circulation in the Nordic Seas and Arctic Ocean estimated from simplified dynamics. Journal of Marine Research 61: 175-210.

Robinson, I.S. & J. Johannessen, 1997. Opportunities for combined SAR and ATSR ocean observations during the ERS Tandem Mission. Proceedings of the 3rd ERS Symposium on Space of the service of our Environment, Florence, Italy, 17-21 March 1997, ESA SP 414, Volume 3, 1337-1342.

Ross, T. & R. Lueck, 2003. Sound scattering from oceanic turbulence. Geophysical Research Letters 30(6): 1343, doi:10.1029/2002GL016733.

Shuchman, R.A., D.R. Lyzenga & G.A. Meadows, 1985. Synthetic aperture radar imaging of ocean-bottom topography via tidal-currents interactions: theory and observations. International Journal of Remote Sensing 6: 1179-1200.

Siegel, H. & T. Seifert, 1985. Influence of the sea bottom on the spectral reflectance in the Oder Bank region. Beiträge zur Meereskunde: 52, 65-71.

Smith, P., 1986. Observations of surface currents at Nantucket Shoals and implications for radar imaging of the bottom. Proceedings of IGARSS'86 Symposium, Zürich 8-11 September 1986, ESA SP-254, Published by ESA Publications Division c/o ESTEC, Noordwijk, The Netherlands, 795-800.

Soulsby, R.L., R. Atkins, C.B. Waters & N. Oliver, 1991. Field measurements of suspended sediment over sandwaves. In: Sand Transport in Rivers, Estuaries and the Sea, edited by R. Soulsby and R. Bettess, A.A. Balkema, Rotterdam, 155-162.

Stevenson, R.E., 1999. A view from space: the discovery of nonlinear waves in the ocean's near-surface layer. 21st Century Science & Technology, 12(2): 34-47.

Stewart, H.B. & G.F. Jordan, 1964. Underwater sand ridges on Georges Shoal. In: Papers in Marine Geology, F.P. Shepard Commemorative Volume, R.L. Miller, editor, Macmillan Co., New York, U.S.A., 102-114.

Stolk, A., 2008. Seventy years of sandwave research in the Netherlands. In: Parsons D.R., Garlan T., Best, J.L. (Eds.), Proceedings of the International Workshop on Marine and River Dune Dynamics III, 1-3 April 2008, University of Leeds, Leeds, United Kingdom, 291-295.

Stolte, S., 1990. Dynamics of short waves and wave breaking. Federal Armed Forces Underwater Acoustics and Marine Geophysics Research Institute Kiel, Report 1990-4, 48 pp.

Stolte, S., 1994. Shallow water sonar conditions and radar backscatter. IEEE Journal of Oceanic Engineering 19: 30-35.

Tanimoto, Y., 2003. Discovery of the effect of the Kuroshio Current on the climate around Japan through satellite observation data. Blue Earth 15(2): 22-25.

Valenzuela, G. R., 1978. Theories for the interaction of electromagnetic and ocean waves-A review. Boundary-Layer Meteorology 13: 277-293.

Valenzuela, G.R., D.T. Chen, W.D. Garrett & J.A.C. Kaiser, 1983. Shallow water bottom topography from radar imagery, Nature 303: 687-689.

Van Veen, J., 1936. Onderzoekingen in de Hoofden met betrekking tot de Nederlandsche Kust. Algemeene Landsdrukkerij, 'S-Gravenhage, 252 pp.

Van Veen, J., 1938. Untersuchungen in der Straße von Dover mit dem Vermessungsschiff „Oceaan". International Journal of Earth Sciences 29: 274-286.

Yentsch, C.S., D.A. Phinney & J.W. Campbell, 1994. Color banding on Georges Bank as viewed by coastal zone color scanner. Journal of Geohysical Research 99: 7401-7410.

Zimmerman, J.F.T., 1985. Radar images of the sea bed, Nature 314: 224-226.